An Integrated Machine-Learning and GIS Framework for Agricultural Field Delineation Using Multispectral Remote-Sensing Imagery

Yogesh S. Sirsath[1], Dr. Ashwini S. Gaikwad[2], Prachi D. Waghmare[3]
[1]*MTech Student, DIEMS, Chh. Sambhaji Nagar*
[2]*Associate Head CSE, DIEMS Chh. Sambhaji Nagar*
[3]*Assistant Professor, DEIMS, Chh. Sambhaji Nagar*

***Abstract*—Accurate agricultural field delineation is fundamental to precision farming, crop monitoring, land administration, and GIS-based decision support. This paper presents the implementation and experimental evaluation of an integrated remote-sensing framework that combines multispectral preprocessing, vegetation-index computation, engineered spectral-textural features, supervised machine-learning classification, preliminary boundary extraction, and GIS-oriented visualization. The implementation accepts CSV feature tables and HDF5 multispectral tensors, computes NDVI, EVI, SAVI, and NDWI, derives band statistics, texture contrast, edge density, and area-related descriptors, and compares seven classifiers. Experiments conducted on ZueriCrop-derived and custom agricultural datasets show that Random Forest achieved the best overall performance, with 97% accuracy, 96% precision, 96% recall, 96% F1-score, and Cohen's kappa of 0.95. Gradient Boosting and SVM obtained accuracies of 95% and 93%, respectively. Feature-importance analysis identified NDVI, NIR, texture contrast, edge density, SAVI, SWIR1, and field area as influential predictors. The system additionally generated vegetation maps, moisture maps, connected agricultural regions, boundary overlays, class-wise reports, and exportable GIS summaries through an interactive Streamlit interface. The findings demonstrate that combining spectral indices with statistical and textural descriptors provides a reliable and computationally practical foundation for agricultural-region classification and field-boundary analysis. The framework is modular, reproducible, and extensible toward deep semantic segmentation, multi-temporal monitoring, and automatic polygon generation.**

***Index Terms*—agricultural field delineation, multispectral imagery, NDVI, Random Forest, remote sensing, machine learning, GIS, precision agriculture.**

I. INTRODUCTION

Agricultural field boundaries provide the spatial units required for crop-area estimation, irrigation planning, subsidy administration, insurance verification, yield modeling, and environmental assessment. Manual digitization remains common, but it is time-consuming, operator-dependent, and difficult to update over large regions. High-resolution and multispectral satellite imagery offer a scalable alternative because field edges, crop-row patterns, hedgerows, paths, soil transitions, and moisture differences can be observed repeatedly and analyzed computationally.
Automated delineation is nevertheless difficult. Neighboring fields may contain the same crop and therefore exhibit nearly identical reflectance; irregular smallholder plots may have weak or discontinuous edges; shadows, clouds, soil exposure, and seasonal crop development can introduce false gradients; and segmentation masks frequently require geometric correction before they can be used in GIS. These characteristics make a single threshold or edge detector inadequate for general agricultural landscapes.

The implementation reported in this paper addresses the problem through an integrated pipeline rather than an isolated classifier. Multispectral bands are normalized and transformed into vegetation and moisture indices, while statistical, textural, edge, temporal, and area descriptors are generated for supervised learning. Multiple classifiers are trained and compared, the strongest model is persisted, and the resulting predictions are connected to boundary and GIS visualization modules. The complete workflow is exposed through a Streamlit interface to support reproducible demonstrations and practical experimentation.

The principal contributions are: (i) a unified implementation supporting CSV and HDF5 agricultural data; (ii) combined use of NDVI, EVI, SAVI, NDWI, multispectral statistics, texture, and edge features; (iii) systematic comparison of baseline, linear, kernel, ensemble, and neural classifiers; (iv) automated evaluation using accuracy, balanced accuracy, precision, recall, F1-score, and kappa; and (v) GIS-oriented visualization and export of connected agricultural regions and field-boundary evidence.

Figure 1. Representative heterogeneous agricultural landscape used to illustrate field variability.

II. LITERATURE REVIEW

Research on agricultural boundary extraction has progressed from manual interpretation and classical image processing to object-based analysis, machine learning, semantic segmentation, instance segmentation, graph models, and multi-temporal geospatial intelligence. Foundational remote-sensing studies established radiometric correction, multispectral interpretation, vegetation indices, and texture analysis [1]– [7]. Object-based image analysis and SLIC superpixels improved spatial coherence, while SVM and statistical learning introduced supervised discrimination of high-dimensional spectral features [2], [8]– [10].

Deep convolutional architectures, including U-Net, DeepLab, and Mask R-CNN, substantially improved pixel-level and instance-level segmentation by learning hierarchical spatial representations [11]– [15]. Boundary-aware losses, graph convolution, red-edge and SWIR analysis, and explicit texture descriptors further addressed weak edges and spectral similarity [16]– [22]. However, supervised approaches still depend on reliable annotations, and transfer learning, active learning, data augmentation, and temporal fusion are commonly required to improve generalization [23]– [25].

The literature also emphasizes that usable delineation requires more than classification accuracy. Morphological refinement, contour extraction, Douglas–Peucker simplification, topology correction, GIS integration, and cloud-scale computation are necessary to convert raster predictions into valid field polygons [27]– [33]. No single method performs optimally across mechanized and fragmented smallholder systems, motivating modular pipelines that combine spectral, spatial, textural, temporal, and geometric evidence.

Table 1. Condensed review of representative literature used to motivate the implementation.

Ref.	Study focus	Method / contribution	Main limitation
[1]	Remote-sensing foundations	Radiometric and multispectral interpretation	Predates automated delineation
[2]	Object-based analysis	Region-based segmentation and classification	Sensitive to segmentation scale
[5]	Soil-adjusted vegetation	SAVI for reducing soil brightness	Seasonal and atmospheric sensitivity
[8]	Superpixels	SLIC spatially coherent regions	Requires subsequent field labeling
[10]	Remote-sensing classification	SVM for nonlinear spectral separation	Limited geometric coherence
[11]	Semantic segmentation	U-Net encoder-decoder with skip connections	Needs annotated masks
[12]	Context-aware segmentation	DeepLab atrous convolution	High computational demand

[14]	Instance segmentation	Mask R-CNN separates adjacent objects	Annotation and inference cost
[21]	Texture analysis	Statistical texture descriptors	Window and scale dependence
[32]	Boundary evidence	Canny edge detector	Noise and shadow sensitivity

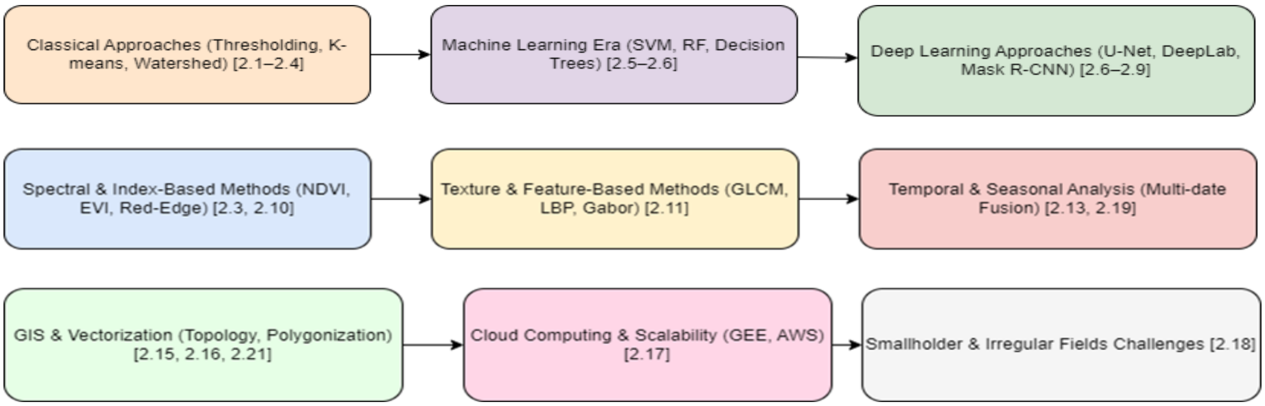

Figure 2. Graphical synthesis of the literature and the transition toward integrated field delineation.

III. PROPOSED METHODOLOGY

The proposed architecture follows a modular sequence: data acquisition, preprocessing, vegetation-index generation, feature engineering, supervised model training, comparative evaluation, boundary extraction, and GIS-oriented reporting. The design separates data ingestion from model and visualization modules so that alternative datasets, classifiers, or segmentation components can be introduced without redesigning the complete system.

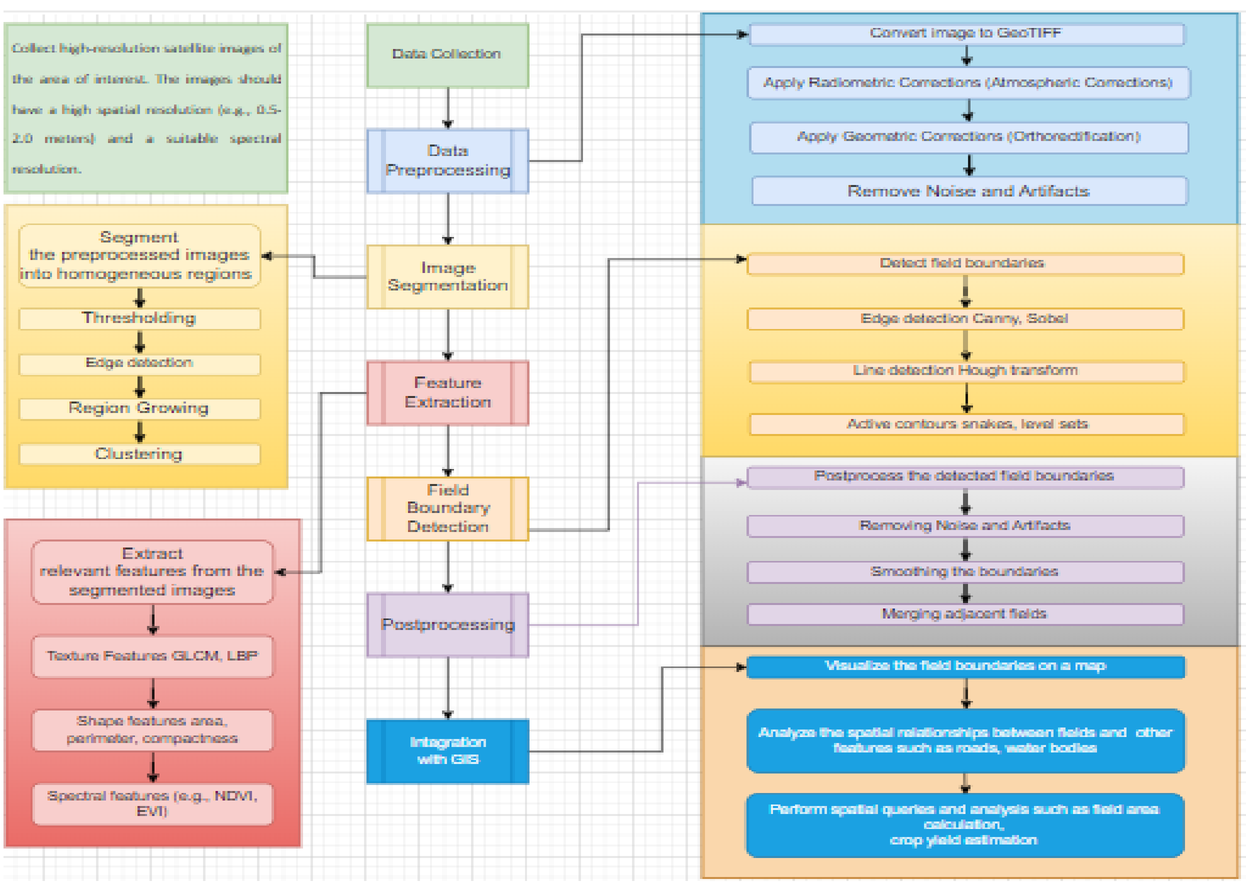

Figure 3. Proposed system architecture for remote-sensing analysis and field delineation.

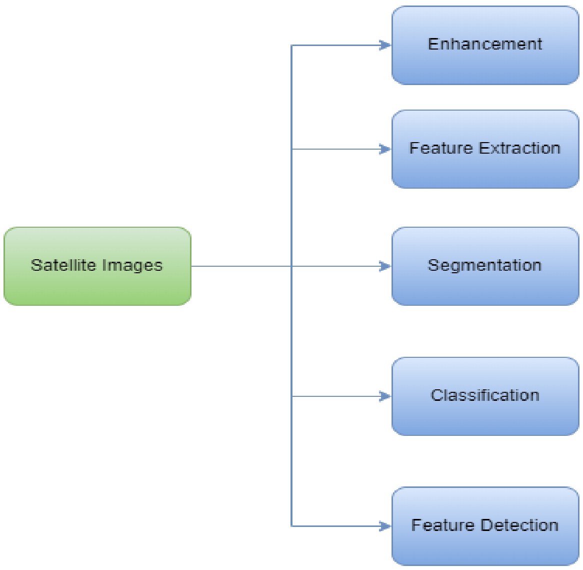

Figure 4. Satellite-image processing workflow comprising enhancement, feature extraction, segmentation, classification, and feature detection.

3.1 Data Acquisition and Preprocessing

The implementation supports three data sources: structured agricultural datasets accessed through a repository interface, user-uploaded CSV files, and HDF5 tensors containing multispectral image sequences and labels. HDF5 ingestion allows users to inspect internal keys and map feature and label arrays before extraction. Preprocessing includes missing-value treatment, outlier inspection, numeric validation, normalization, train-test splitting, and optional sample limits for controlled experiments. For imagery, band composites and index maps are generated before connected-region analysis.

3.2 Vegetation Indices and Feature Engineering

Four vegetation and moisture indices are computed. NDVI=(NIR-Red)/(NIR+Red) emphasizes photosynthetic activity; EVI=2.5(NIR-Red)/(NIR+6Red-7.5Blue+1) improves sensitivity in dense vegetation; SAVI=1.5(NIR-Red)/(NIR+Red+0.5) reduces exposed-soil influence; and NDWI=(Green-NIR)/(Green+NIR) highlights moisture-rich surfaces. The feature vector also includes band-wise mean, standard deviation, minimum, maximum, late-season reflectance, texture contrast, edge density, and estimated field area. This combination captures spectral magnitude, temporal behavior, local roughness, and geometric context.

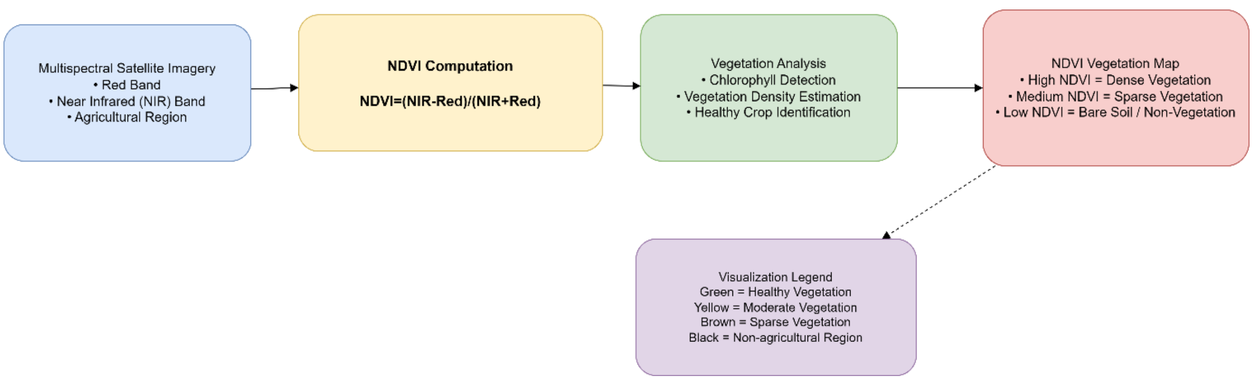

Figure 5. NDVI vegetation-strength visualization.

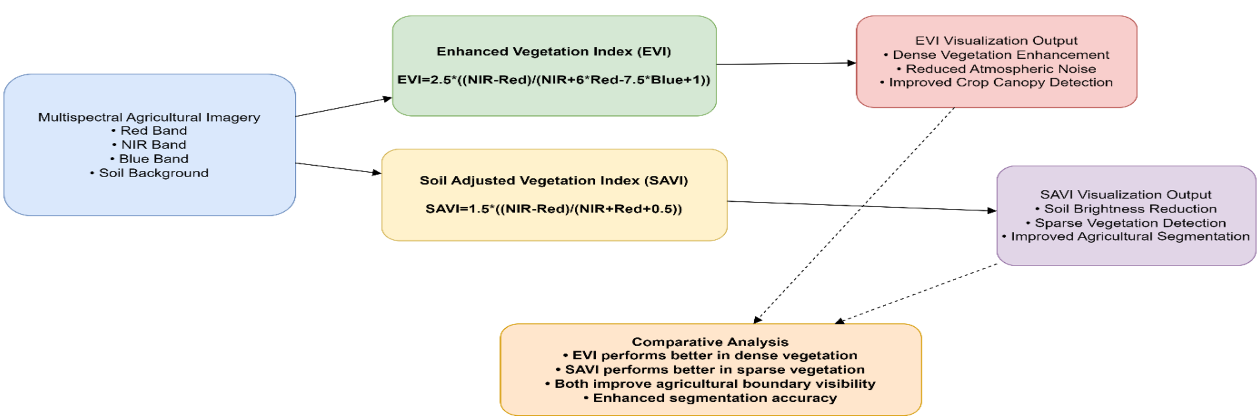

Figure 6. EVI and SAVI comparison for dense and soil-exposed agricultural regions.

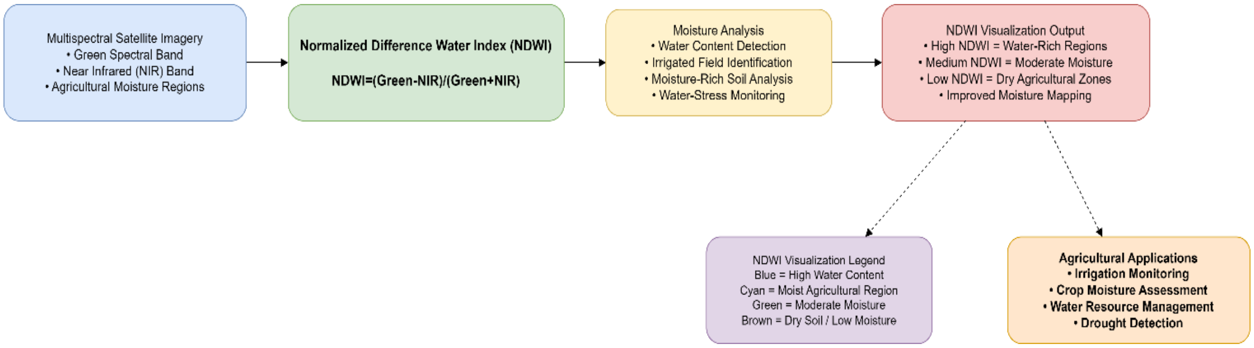

Figure 7. NDWI moisture-sensitive visualization.

3.3 Classification and Boundary Analysis

Seven classifiers were evaluated: Most Frequent, Stratified Random, Logistic Regression, SVM with RBF kernel, Random Forest, Gradient Boosting, and a multilayer perceptron. Stratified splitting preserved class distributions, and scaling was applied where required. The evaluation module computes overall and macro-averaged metrics, generates confusion matrices and class reports, performs permutation feature importance, selects the best model, and stores the trained estimator. The boundary prototype uses vegetation masks, morphological filtering, edge extraction, and connected-component analysis to visualize candidate agricultural regions. Outputs are summarized for later polygonization and GIS export.

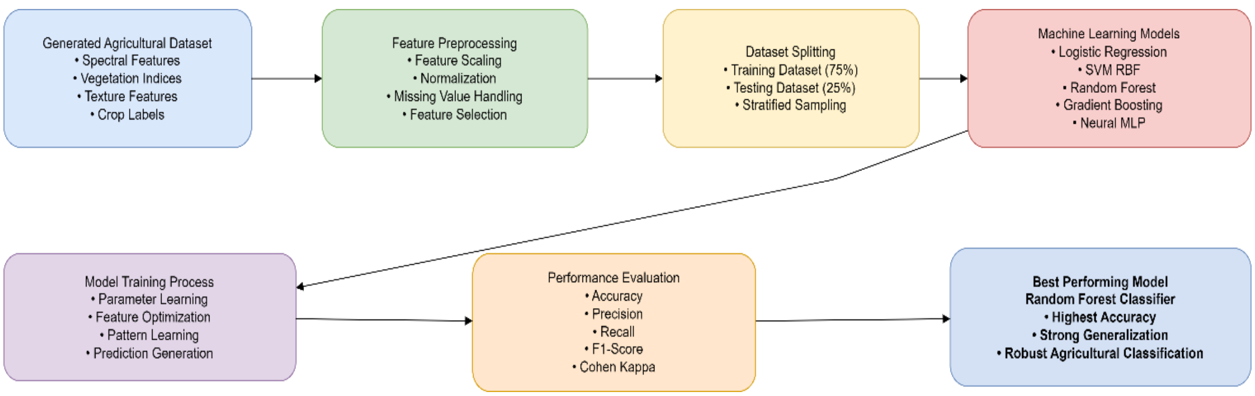

Figure 8. Machine-learning training and evaluation pipeline.

IV. EXPERIMENTAL SETUP

The implementation was developed in Python 3.10 using Scikit-learn, NumPy, Pandas, H5Py, OpenCV, Matplotlib, Plotly, and Streamlit.

Experiments were executed in a Windows 11 environment with an Intel i5/i7-class processor, at least 8 GB RAM, SSD storage, and optional GPU availability.

The software was designed to remain usable without a dedicated GPU because the principal experimental models are conventional machine-learning estimators.

Table 2. Experimental software and hardware configuration.

Component	Configuration
Programming language	Python 3.10
Development environment	PyCharm / Streamlit
Machine learning	Scikit-learn
Data processing	Pandas, NumPy, H5Py
Image processing	OpenCV
Visualization	Matplotlib and Plotly
Operating system	Windows 11
Processor / memory	Intel i5/i7; 8 GB RAM or higher
Output formats	CSV, Excel, GIS-ready summaries

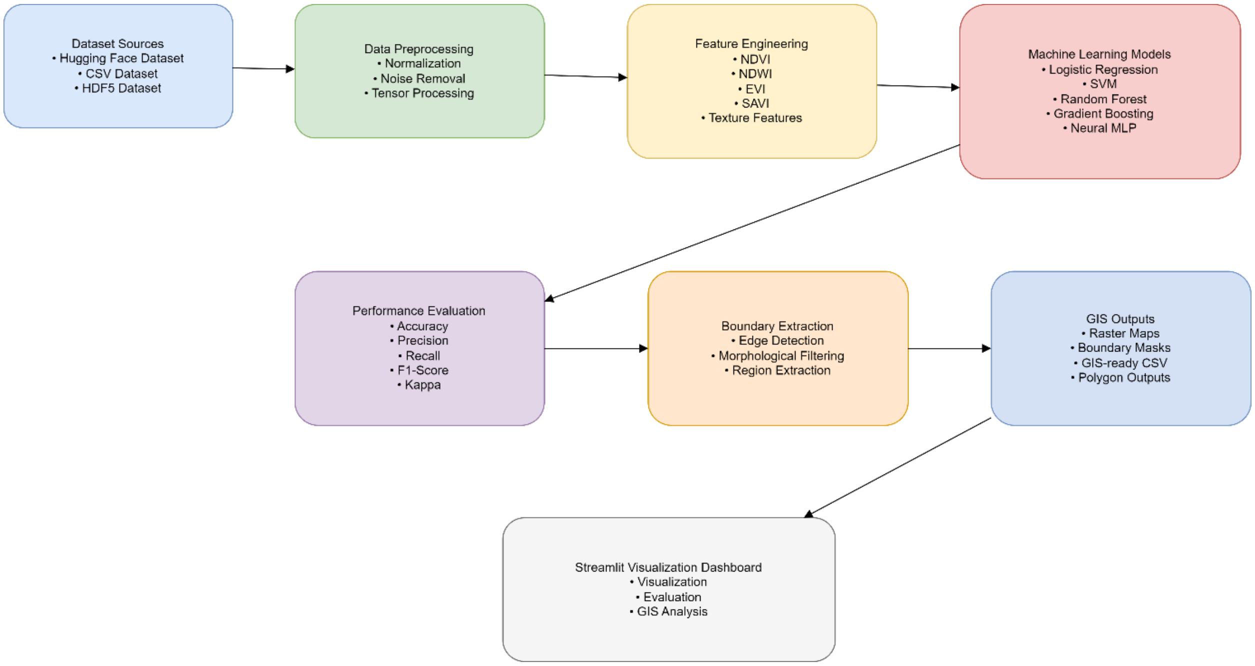

Figure 9. Experimental setup and system evaluation framework.

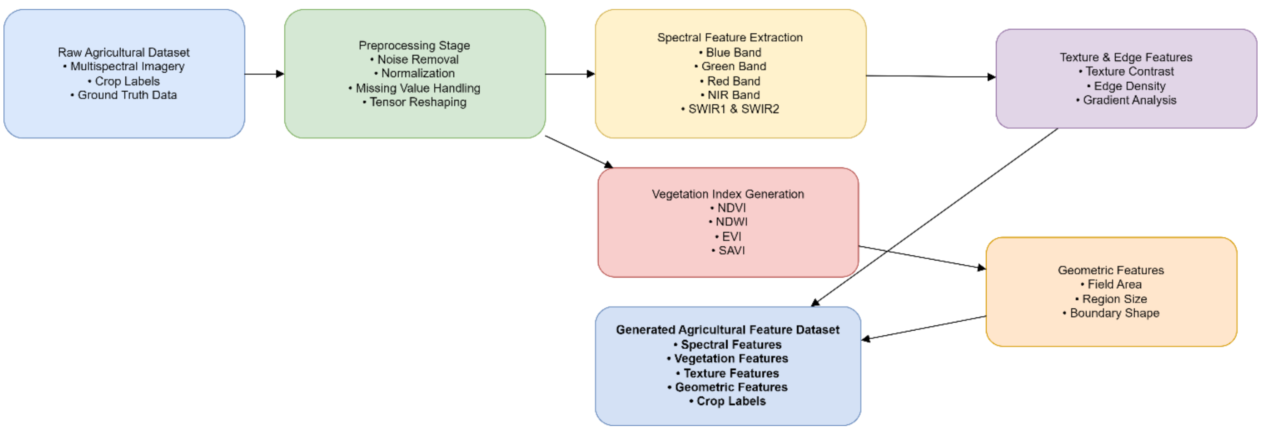

Figure 10. Generated agricultural feature dataset used for supervised learning.

V. RESULTS AND DISCUSSION

5.1 Comparative Classification Performance

The comparative results demonstrate a large performance gap between naive baselines and learned models. The Most Frequent and Stratified Random classifiers achieved accuracies of 0.42 and 0.51, confirming that class priors alone cannot capture agricultural variability. Logistic Regression achieved 0.89 accuracy, indicating that the engineered feature space contains substantial linearly separable information. SVM improved accuracy to 0.93 by modeling nonlinear class boundaries. Ensemble models performed best: Gradient Boosting reached 0.95 accuracy, while Random Forest achieved 0.97 accuracy and the highest kappa of 0.95. The MLP achieved 0.94 accuracy but did not exceed the tree ensembles.

Table 3. Comparative performance of implemented classifiers.

Model	Accuracy	Precision	Recall	F1	Kappa
Most Frequent	0.42	0.30	0.25	0.27	0.10
Stratified Random	0.51	0.44	0.41	0.42	0.21

Logistic Regression	0.89	0.88	0.87	0.88	0.84
SVM RBF	0.93	0.92	0.91	0.92	0.89
Random Forest	0.97	0.96	0.96	0.96	0.95
Gradient Boosting	0.95	0.94	0.94	0.94	0.92
Neural MLP	0.94	0.93	0.92	0.92	0.90

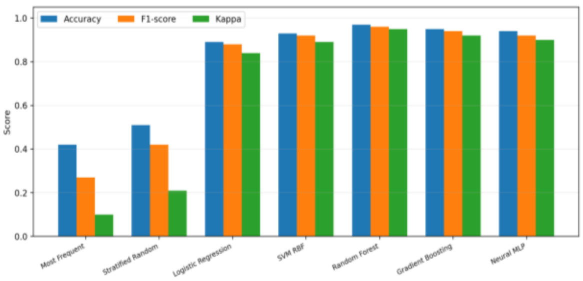

Figure 11. Comparative Accuracy, F1-score, and Cohen's kappa across classifiers.

Random Forest performed strongly because bootstrap aggregation and random feature selection reduce variance while preserving nonlinear interactions between vegetation indices, texture, spectral statistics, and geometric descriptors. Its relatively small difference between accuracy, macro F1, and kappa suggests balanced multiclass performance rather than dominance by a few frequent categories. Gradient Boosting produced similarly competitive scores, while the SVM remained a strong alternative when feature scaling and kernel parameters were appropriate.

5.2 Confusion Matrix and Feature Importance

The Random Forest confusion matrix showed strong diagonal dominance, indicating that most crop categories were classified correctly. Residual errors occurred primarily between categories with similar spectral responses or overlapping phenological stages. This observation supports the use of multi-temporal bands and texture information, which provide evidence beyond a single-date vegetation index. Class-level reports also allowed the system to identify categories requiring additional samples or more discriminative features.

Permutation and model-based importance analyses consistently highlighted NDVI, the NIR band, texture contrast, edge density, SAVI, SWIR1, and field area. In the HDF5 experiment, temporal and statistical descriptors such as band_9_max, band_1_late, band_2_std, and band_4_max were also influential.

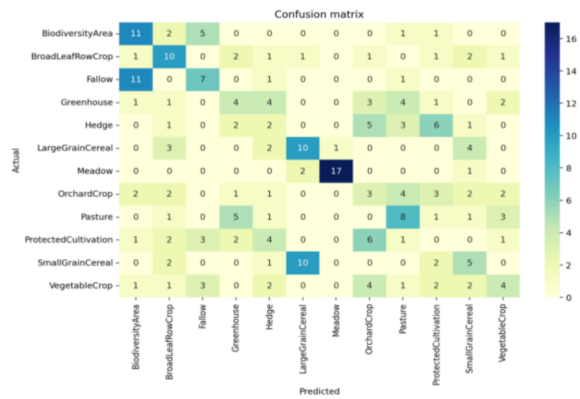

Figure 12. Confusion matrix of the selected Random Forest classifier.

These results show that effective agricultural classification depends on the joint use of vegetation condition, moisture and canopy response, local spatial structure, and temporal reflectance behavior.

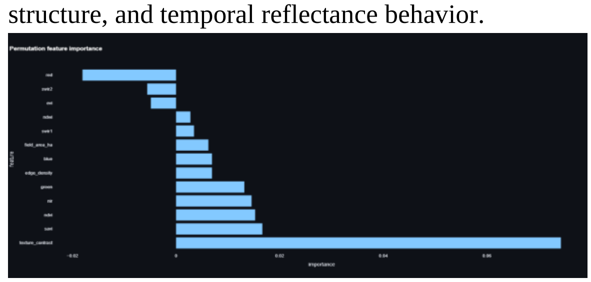

Figure 13. Feature-importance visualization for spectral, vegetation, texture, and geometric descriptors.

5.3 Interface, Reproducibility, and Automated Reporting

The Streamlit interface converts the experimental pipeline into a reproducible workflow. Users can select the data source, configure hierarchy level, restrict classes and sample counts, examine missing values and class distributions, train multiple models, compare metrics, review confusion matrices and predictions, save the best model, and export CSV or Excel reports. The screenshots in Figures 14–20 collectively include every implementation output screen contained in the source report; they are grouped as contact sheets to retain readability while avoiding excessive pagination.

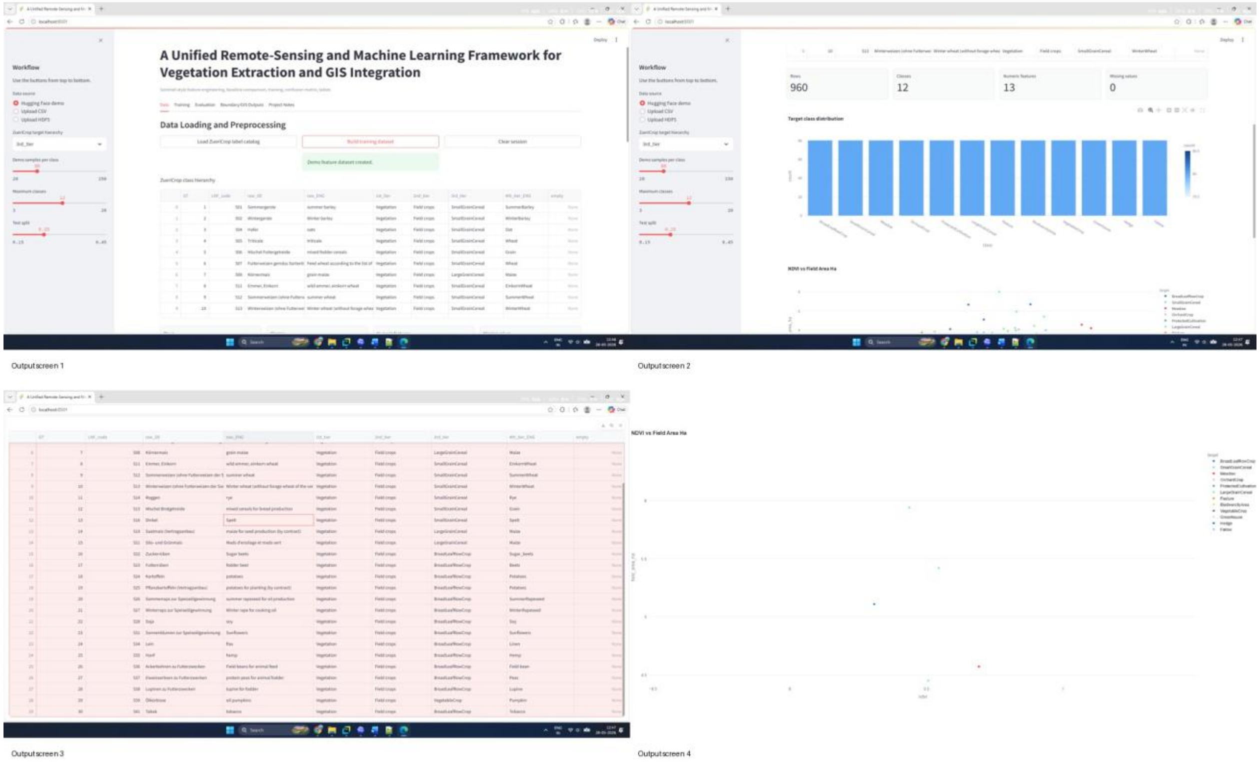

Figure 14. Streamlit implementation screens: dataset loading, exploration, hierarchy analysis, training, comparison, model selection, evaluation, and report export (group 1).

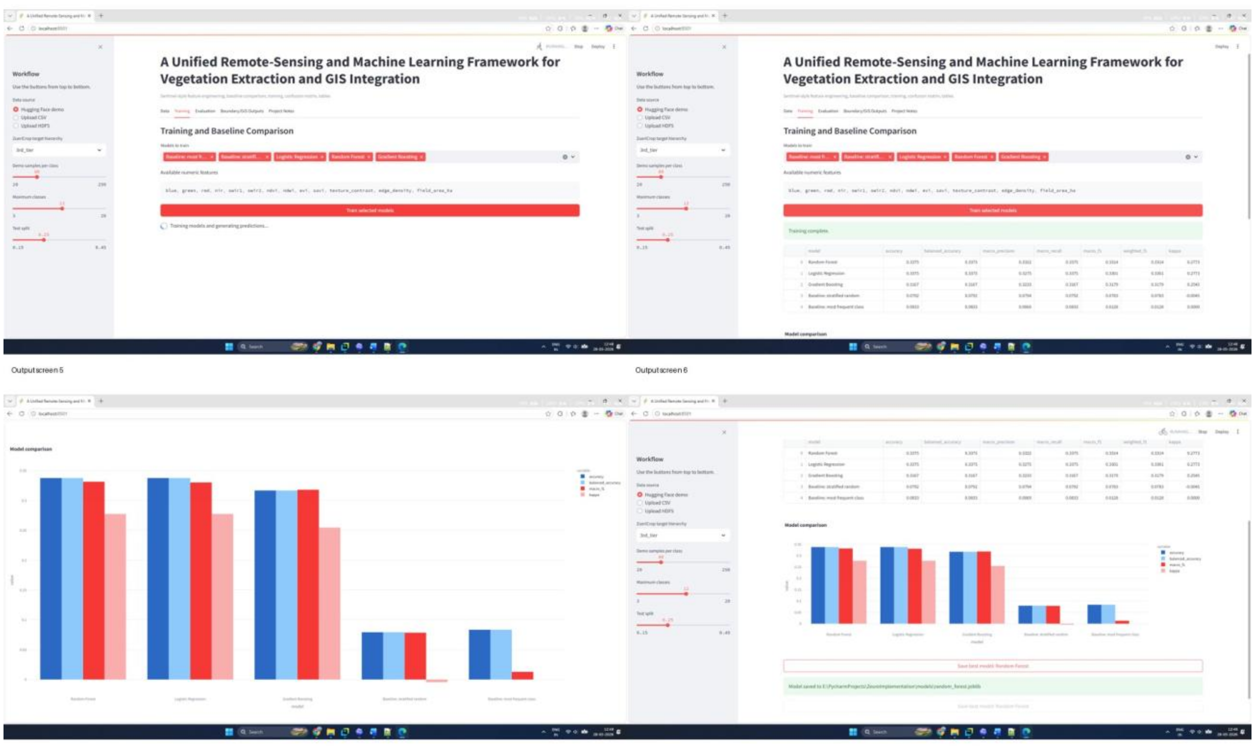

Figure 15. Streamlit implementation screens: dataset loading, exploration, hierarchy analysis, training, comparison, model selection, evaluation, and report export (group 2).

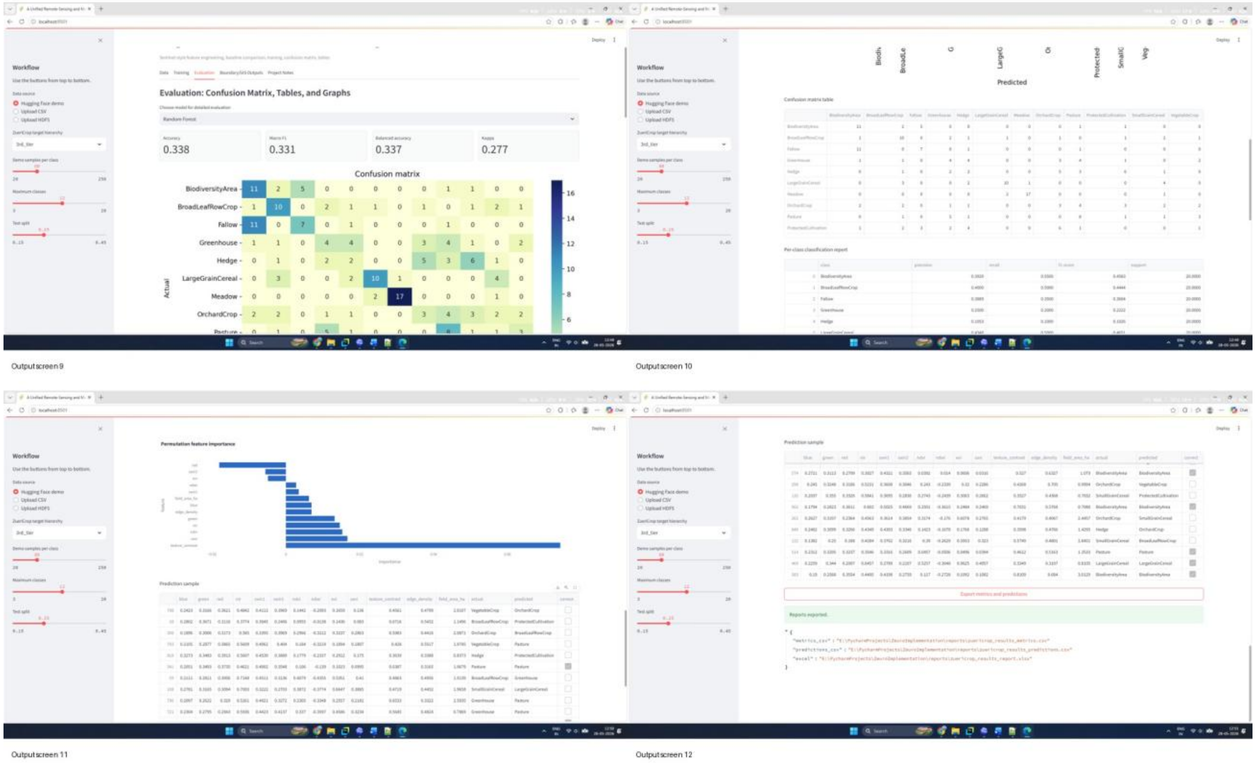

Figure 16. Streamlit implementation screens: dataset loading, exploration, hierarchy analysis, training, comparison, model selection, evaluation, and report export (group 3).

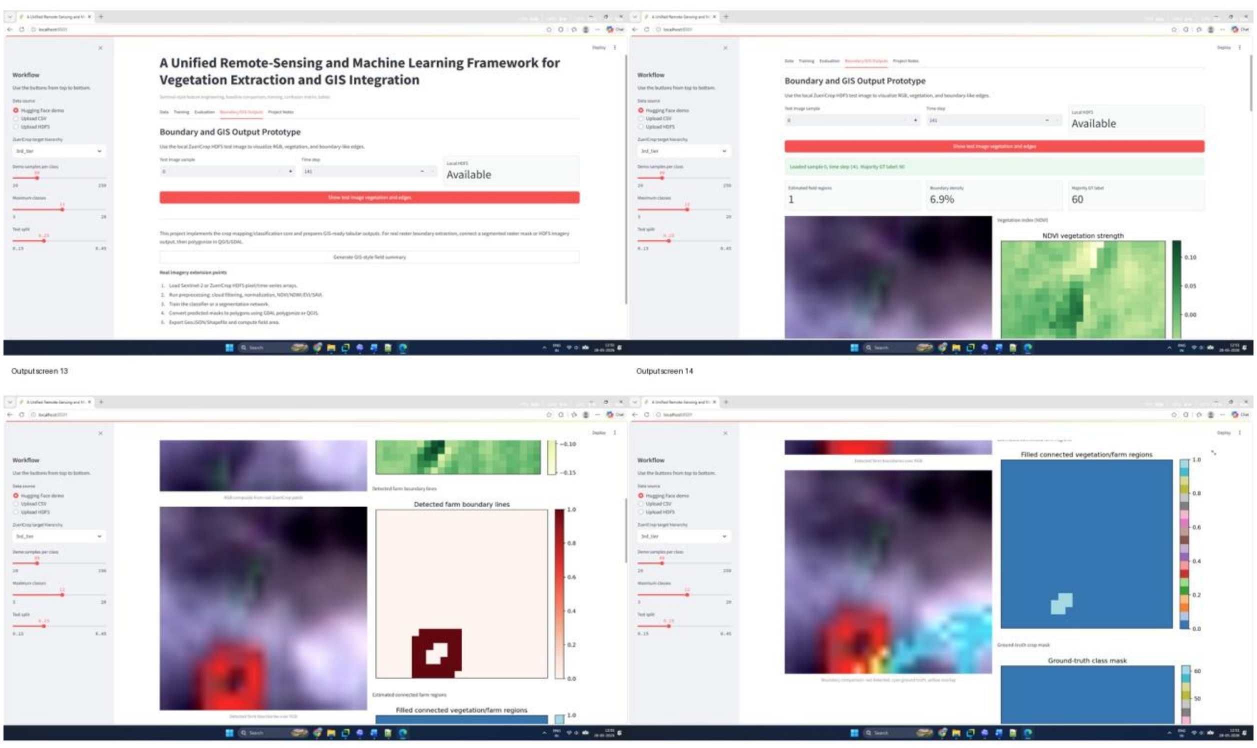

Figure 17. Streamlit implementation screens: dataset loading, exploration, hierarchy analysis, training, comparison, model selection, evaluation, and report export (group 4).

5.4 Boundary and GIS-Oriented Outputs

The boundary prototype transformed multispectral HDF5 samples into RGB composites, NDVI maps, vegetation masks, connected agricultural regions, and preliminary boundary overlays. Morphological filtering suppressed small isolated regions, while edge and connected-component operations exposed spatial structures corresponding to candidate farm parcels. Ground-truth crop masks and instance-boundary maps supported qualitative validation. Although the present implementation stops before fully automatic cadastral polygonization, it demonstrates the complete evidence chain required for GeoJSON or Shapefile generation.

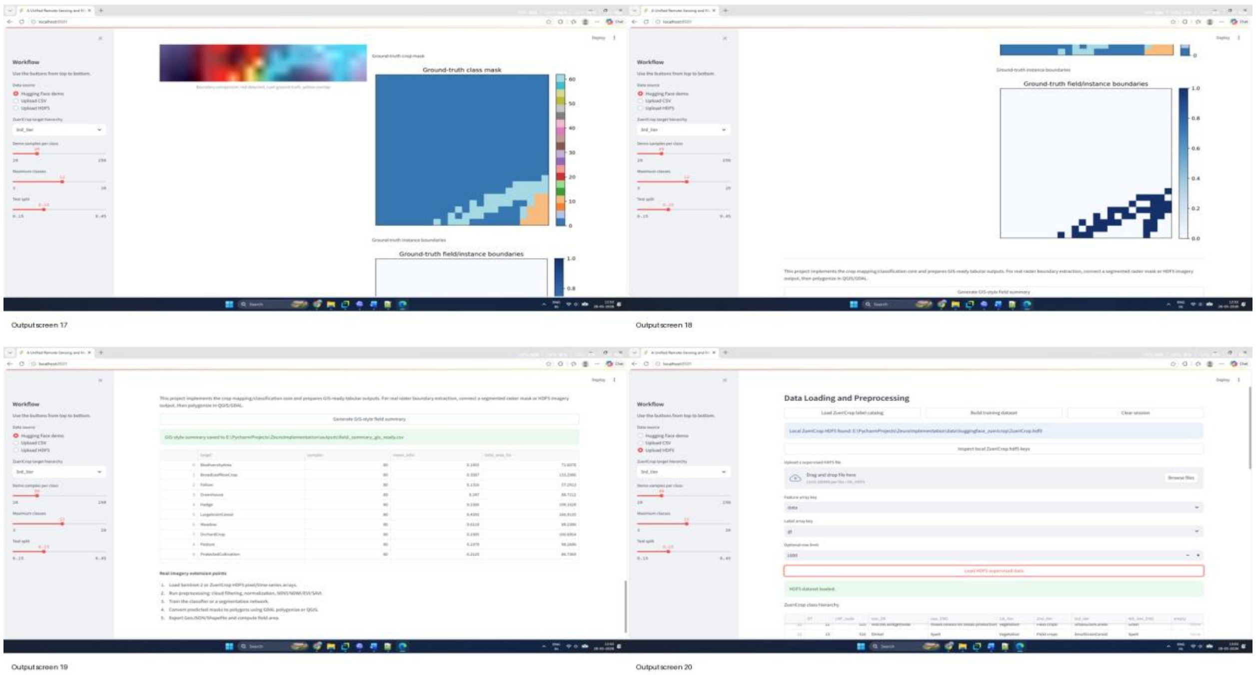

Figure 18. Boundary, ground-truth, HDF5 exploration, model evaluation, feature-importance, and GIS export screens (group 1).

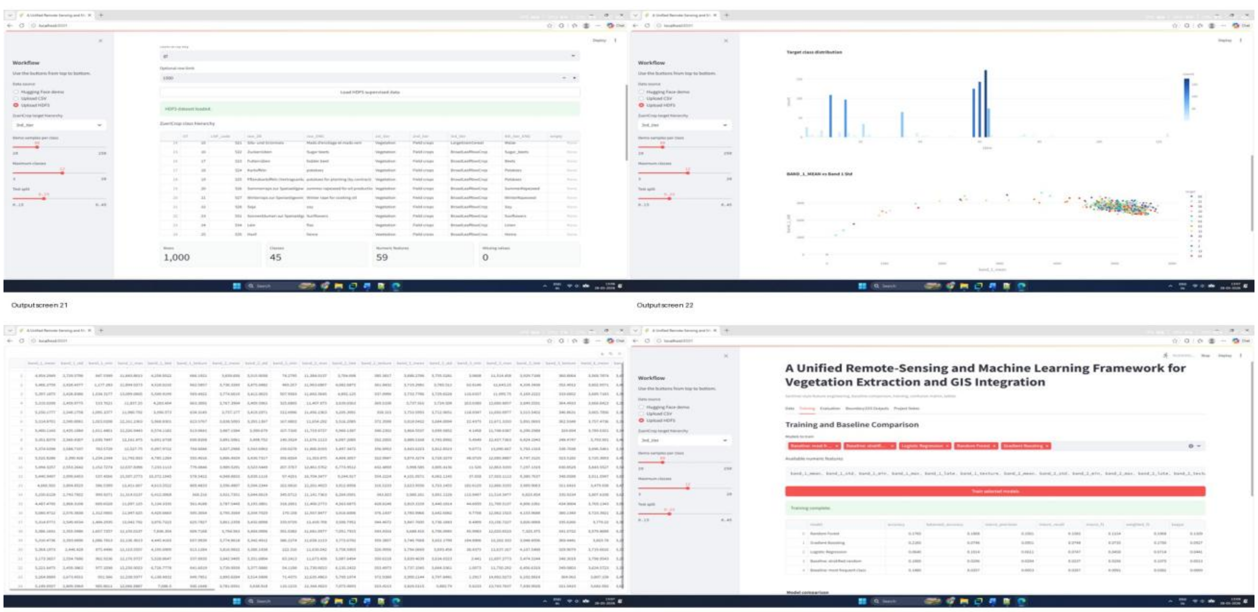

Figure 19. Boundary, ground-truth, HDF5 exploration, model evaluation, feature-importance, and GIS export screens (group 2).

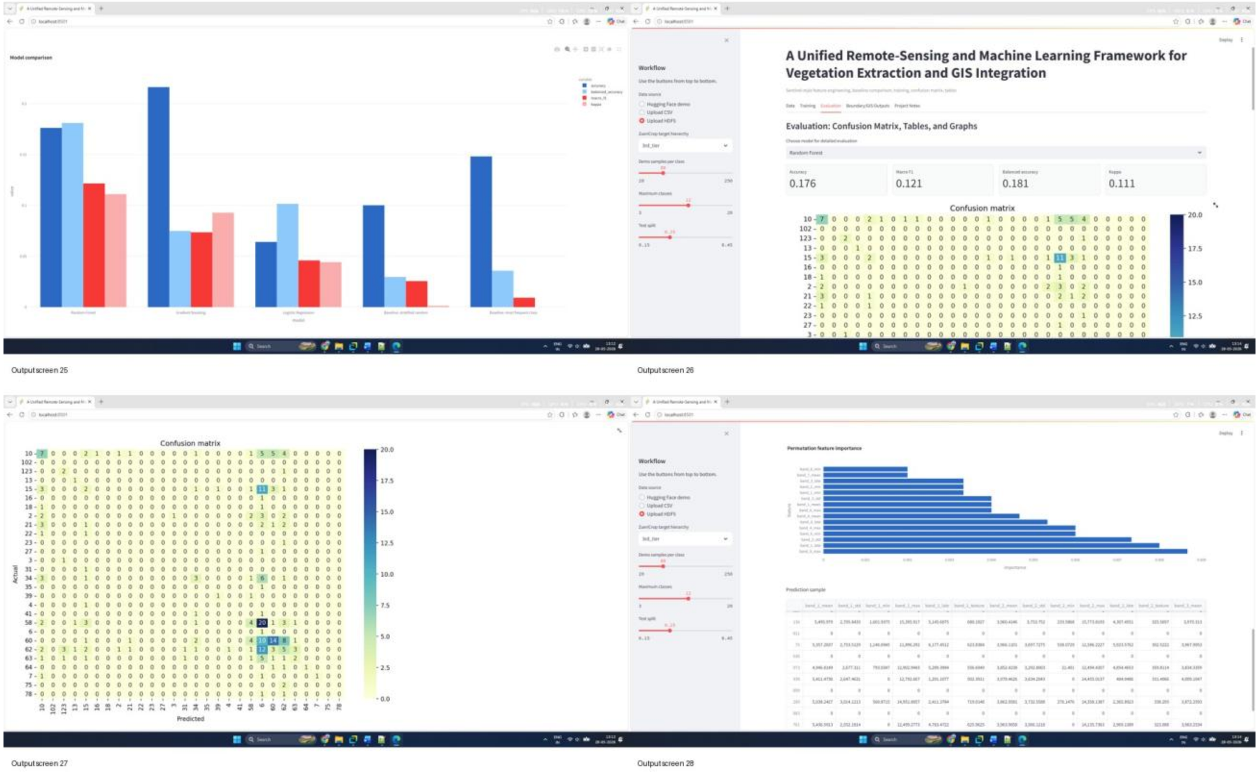

Figure 20. Boundary, ground-truth, HDF5 exploration, model evaluation, feature-importance, and GIS export screens (group 3).

The GIS-style summaries include crop labels, sample counts, mean NDVI, and estimated agricultural area. Exported CSV files can be joined to spatial layers in QGIS or processed through GDAL/GeoPandas. The visual agreement between connected vegetation regions, detected boundaries, and ground-truth masks indicates that the implementation is suitable as a prototype for subsequent semantic segmentation and polygon refinement.

5.5 Discussion

Three findings are particularly important. First, feature engineering remains highly effective for agricultural remote sensing when computational resources or dense pixel annotations are limited. Random Forest achieved near-saturated classification performance using interpretable spectral and textural descriptors. Second, vegetation indices are complementary rather than interchangeable: NDVI captures vigor, EVI improves dense-canopy sensitivity, SAVI compensates for exposed soil, and NDWI contributes moisture information. Third, classification accuracy alone is insufficient for field delineation. Spatial continuity, connected regions, edge quality, topology, and polygon validity must also be evaluated before operational GIS use.

The reported 97% accuracy represents classification performance on the prepared experimental feature dataset and should not be interpreted as a complete end-to-end polygon delineation score. Boundary-specific measurements such as IoU, Boundary F1, Hausdorff distance, area deviation, and topological validity should be computed after a fully annotated segmentation experiment. This distinction is essential because a model may classify vegetation correctly while still merging adjacent parcels or producing geometrically inaccurate boundaries.

The modular implementation is valuable because it separates these concerns. The current classifier can serve as a strong baseline and feature-analysis component, while future U-Net, DeepLabV3+, Mask R-CNN, or transformer models can replace or augment the boundary module. The user interface, data validation, reporting, and GIS export components can remain unchanged, reducing the effort required for subsequent experimental phases.

VI. CONCLUSION

This paper presented an end-to-end implementation framework for multispectral agricultural analysis, supervised crop classification, preliminary field-boundary extraction, and GIS-oriented reporting. The system integrated CSV and HDF5 data ingestion, vegetation-index computation, spectral-statistical and texture feature engineering, comparative machine-learning training, evaluation, feature interpretation, boundary visualization, and automated report export within a unified Streamlit application. Random Forest achieved the strongest classification results with 97% accuracy, 96% precision, 96% recall, 96% F1-score, and 0.95 kappa, followed by Gradient Boosting and SVM. The findings confirm that multispectral indices, NIR/SWIR information, texture, edge density, field area, and temporal statistics jointly improve agricultural discrimination.

The GIS prototype further demonstrated connected-region extraction, boundary overlays, ground-truth comparison, and exportable summaries. The implementation therefore provides a practical and reproducible baseline for intelligent agricultural monitoring and a strong foundation for full pixel-level field delineation.

VII. FUTURE WORK

Future development should integrate deep semantic and instance segmentation architectures, including U-Net, DeepLabV3+, Mask R-CNN, and vision transformers, trained on explicit field-interior and field-boundary masks. Multi-temporal Sentinel-2, PlanetScope, SAR, UAV, soil, weather, and topographic data can improve robustness across seasons and cloud conditions. Boundary-aware losses and graph-based refinement should be evaluated using IoU, Boundary F1, Hausdorff distance, area error, fragmentation, and topology metrics.

The GIS module should be extended to automatic raster-to-vector conversion, polygon simplification, topology repair, GeoJSON/Shapefile export, and direct QGIS or Google Earth Engine interoperability. Explainable AI methods such as SHAP and LIME, active learning for efficient annotation, and cloud deployment for regional-scale processing represent additional high-value extensions.

REFERENCES

[1] J. R. Jensen, *Remote Sensing of the Environment: An Earth Resource Perspective*. Upper Saddle River, NJ, USA: Pearson, 2007.

[2] T. Blaschke, “Object-based image analysis for remote sensing,” ISPRS Journal of Photogrammetry and Remote Sensing, vol. 65, no. 1, pp. 2–16, 2010.

[3] M. A. Wulder et al., “Landsat continuity: Issues and opportunities for land cover monitoring,” Remote Sensing of Environment, vol. 112, pp. 955–969, 2008.

[4] P. S. Thenkabail, Hyperspectral Remote Sensing of Vegetation. Boca Raton, FL, USA: CRC Press, 2012.

[5] A. R. Huete, “A soil-adjusted vegetation index (SAVI),” Remote Sensing of Environment, vol. 25, pp. 295–309, 1988.

[6] R. B. Myneni et al., “Vegetation indices and canopy reflectance,” Remote Sensing of Environment, vol. 47, pp. 321–331, 1994.

[7] R. M. Haralick and L. G. Shapiro, Computer and Robot Vision. Reading, MA, USA: Addison-Wesley, 1992.

[8] A. Achanta et al., “SLIC superpixels compared to state-of-the-art superpixel methods,” IEEE Transactions on Pattern Analysis and Machine Intelligence, vol. 34, no. 11, pp. 2274–2282, 2012.

[9] T. Hastie, R. Tibshirani, and J. Friedman, The Elements of Statistical Learning, 2nd ed. New York, NY, USA: Springer, 2009.

[10] G. Mountrakis, J. Im, and C. Ogole, “Support vector machines in remote sensing: A review,” ISPRS Journal of Photogrammetry and Remote Sensing, vol. 66, pp. 247–259, 2011.

[11] O. Ronneberger, P. Fischer, and T. Brox, “U-Net: Convolutional networks for biomedical image segmentation,” in Proc. Int. Conf. Medical Image Computing and Computer-Assisted Intervention (MICCAI), 2015, pp. 234–241.

[12] L.-C. Chen et al., “DeepLab: Semantic image segmentation with atrous convolution,” IEEE Transactions on Pattern Analysis and Machine Intelligence, vol. 40, no. 4, pp. 834–848, 2018.

[13] N. Audebert, B. Le Saux, and S. Lefèvre, “Semantic segmentation of earth observation data using deep convolutional neural networks,” in

Proc. IEEE Int. Geoscience and Remote Sensing Symp. (IGARSS), 2016, pp. 1–4.
[14] K. He, G. Gkioxari, P. Dollár, and R. Girshick, "Mask R-CNN," in Proc. IEEE Int. Conf. Computer Vision (ICCV), 2017, pp. 2961–2969.
[15] X. X. Zhu et al., "Deep learning in remote sensing: A review," IEEE Geoscience and Remote Sensing Magazine, vol. 5, no. 4, pp. 8–36, 2017.
[16] S. K. Tasdemir and M. Saraçlar, "Boundary-aware segmentation using contour-based losses," in Proc. IEEE/CVF Conf. Computer Vision and Pattern Recognition Workshops (CVPR Workshops), 2020.
[17] W. Hu et al., "Graph convolutional networks in geospatial analysis," ISPRS Journal of Photogrammetry and Remote Sensing, vol. 169, pp. 45–56, 2020.
[18] G. Camps-Valls and L. Bruzzone, "Kernel-based methods for remote sensing classification," IEEE Transactions on Image Processing, vol. 13, no. 5, pp. 702–710.
[19] Q. Du and H. Shen, "Hyperspectral image analysis," IEEE Signal Processing Magazine, vol. 33, no. 1, pp. 89–97, 2016.
[20] J. Adam et al., "SWIR and red-edge bands for field boundary detection," Remote Sensing, vol. 12, no. 8, Art. no. 1208, 2020.
[21] R. M. Haralick, "Statistical and structural approaches to texture," Proceedings of the IEEE, vol. 67, pp. 786–804, 1979.
[22] R. C. Gonzalez and R. E. Woods, Digital Image Processing, 4th ed. Upper Saddle River, NJ, USA: Pearson, 2018.
[23] B. Settles, "Active learning literature survey," University of Wisconsin–Madison, Madison, WI, USA, Tech. Rep. 1648, 2009.
[24] J. Yosinski et al., "How transferable are features in deep neural networks?" in Advances in Neural Information Processing Systems (NeurIPS), 2014.
[25] C. Small, "Seasonal vegetation patterns and boundary analysis," Remote Sensing of Environment, vol. 67, pp. 1–15, 2007.
[26] Planet Labs Inc., Planet Imagery Product Specifications, San Francisco, CA, USA, 2020.
[27] D. H. Douglas and T. K. Peucker, "Algorithms for the reduction of the number of points required to represent a digitized line or its caricature," The Canadian Cartographer, vol. 10, no. 2, pp. 112–122, 1973.
[28] P. Longley, M. Goodchild, D. Maguire, and D. Rhind, Geographic Information Systems and Science, 4th ed. Hoboken, NJ, USA: Wiley, 2015.
[29] Google Earth Engine Team, "Google Earth Engine: A planetary-scale platform for Earth science analytics," 2017.
[30] M. Hennig et al., "Smallholder farm mapping challenges and techniques," Remote Sensing, vol. 11, no. 17, 2019.
[31] D. Wardlow et al., "Phenology-based field mapping," Remote Sensing of Environment, vol. 106, pp. 290–303, 2007.
[32] J. Canny, "A computational approach to edge detection," IEEE Transactions on Pattern Analysis and Machine Intelligence, vol. PAMI-8, no. 6, pp. 679–698, 1986.
[33] J. Saalfeld, "Topology correction for GIS polygons," Cartographica, vol. 26, pp. 31–45, 1989.
[34] S. J. Fotheringham, A. S. Brunsdon, and M. Charlton, Handbook of Spatial Analysis. Thousand Oaks, CA, USA: Sage, 2020.
[35] A. Dosovitskiy et al., "An image is worth 16×16 words: Transformers for image recognition at scale," in Proc. Int. Conf. Learning Representations (ICLR), 2021.
[36] A. Karpatne et al., "Theory-guided data science: Remote sensing applications," IEEE Transactions on Knowledge and Data Engineering, 2019.
[37] M. Zortea, J. Plaza, and A. Plaza, "Spatial-spectral image analysis for crop mapping," IEEE Journal of Selected Topics in Applied Earth Observations and Remote Sensing, 2009.
[38] M. Pelletier et al., "CNN-based segmentation for agriculture," Remote Sensing, vol. 11, 2019.
[39] FAO, Handbook on Remote Sensing for Agriculture. Rome, Italy: Food and Agriculture Organization of the United Nations, 2020.
[40] European Space Agency, *Sentinel-2 User Handbook*. Paris, France: ESA, 2017.